S. Afr. J. Chem., 2011, **64**, 71–78,
<http://journals.sabinet.co.za/sajchem/>.

Electrical and Optical Properties of Nanosized Perovskite-type $La_{0.5}Ca_{0.5}MO_3$ (M=Co,Ni) prepared using a Sol-Gel Method

Mohammad Yazdanbakhsh[a], Haman Tavakkoli[a] and Seyed Mohammad Hosseini[b,*]

[a]*Department of Chemistry, Faculty of Science, Ferdowsi University of Mashhad, Mashhad 91799, Iran.*

[b]*Materials and Electroceramics Laboratory, Department of Physics, Ferdowsi University of Mashhad, Mashhad 91799, Iran.*

Received 28 March 2011., revised 19 June 2011, accepted 29 June 2011.

ABSTRACT

In this paper the uniform nanopowders of $La_{0.5}Ca_{0.5}CoO_{3-\delta}$ and $La_{0.5}Ca_{0.5}NiO_{3-\delta}$ (LCCO and LCNO) were synthesized from nitrates of the constituent metal ion, citric acid (CA), and ethylene glycol (EG) by the combined citrate-ethylene glycol (EG) method. These nanopowders were also characterized by differential thermal analysis (DTA), X-ray diffraction (XRD), transmission electron microscopy (TEM), SEM-EDX analysis and Brunauer-Emmett-Teller (BET) method. XRD results show that single perovskite phase was completely formed after calcination at 750 °C. Fourier transform infrared (FTIR) spectra were measured for the xerogels and powder samples after calcination. In addition, the TEM images show that the average particle size of nanoparticles is approximately 25–32 nm in diameter. The ultraviolet (UV) spectrum was used to calculate the absorption coefficient (α) as a function of photon energy ($h\upsilon$) and the obtained results indicate that the optical band gap energy (E_g) for LCNO sample is smaller than that of LCCO. Finally, the temperature dependence of the specific resistivity of LCCO and LCNO sintered at 1100 °C was compared and revealed that the resistivity of both compounds decreases exponentially by increasing the temperature.

KEYWORDS

$La_{0.5}Ca_{0.5}MO_3$, perovskite, sol-gel process, nanopowder, optical properties.

1. Introduction

The structure of the $LaMO_3$ perovskite oxide consists of MO_6 and LaO_{12}. $A_{1-x}A_xBO_{3-\delta}$ belongs to the group of perovskite oxides of the ABO_3 structure with a trivalent rare earth in the *A* position (La) and a trivalent metal ion in the *B* position (Co or Ni). When La^{+3} ions in $LaMO_3$ are replaced by earth alkaline ions such as Ca^{+2} to form $La_{1-x}Ca_x(Co, Ni)O_{3-\delta}$, a positive charge can be generated. Since Co^{+z} and Ni^{+z} cations have different oxidation states, the charge neutrality can be maintained by forming the oxygen vacancies and changing in the valence state of the cations. Therefore, these structures have an oxygen deficiency, δ, due to the high oxygen vacancy concentration and can show a good electrical conductivity, catalytic, mechanical, and colossal magnetoresistance (CMR) properties which have attracted a lot of attention.[1–4] Furthermore, perovskite oxide, $La_{1-x}Ca_x(Co, Ni)O_{3-\delta}$, could be a mixed ionic and electronic conductor. It has been widely investigated for use in various high-temperature electrochemical devices such as solid oxide fuel cells[5–7] or oxygen permeation membranes.[8] Moreover, they have been proposed as alternative catalysts for oxidation of carbon monoxide and hydrocarbons.[9,10]

To investigate the stability of the perovskite-type compounds, ABO_3, Goldschmit introduced the tolerance factor (*t*) by the following equation:

$$t = \frac{r_A + r_O}{\sqrt{2}(r_B + r_O)}, \quad (1)$$

where r_A, r_B and r_O are the radii of the *A* and *B* cations and oxygen ion, respectively.[11] For tolerance factors less than unity, two types of distortion from the cubic structure, the rhombohedral and orthorhombic structures, commonly occur.[12]

* To whom correspondence should be addressed. E-mail: sma_hosseini@yahoo.com

A number of approaches such as solid-state reactions,[13] mechanical-synthesis,[14] coprecipitation,[15,16] solution combustion or thermal decomposition,[17–19] hydro-thermal, the Pechini method and sol-gel technique[20,21] have been used to synthesize $LaMO_3$-based perovskite powders. The Pechini method is highly attractive because various metal ions are chelated to form metal complexes in solution and are uniformly distributed at the molecular level. In Pechini method, citric, oxalic and fatty acids and EDTA (ethylenediaminetetraacetic acid) have been utilized as complexing agents, among which, citric acid is a good chelating agent for transition metal cations and the combined citrate-EG method[22,23] is particularly useful for synthesizing ultra-fine powders of complex oxide compositions.

In the present study, $La_{0.5}Ca_{0.5}CoO_{3-\delta}$ and $La_{0.5}Ca_{0.5}NiO_{3-\delta}$ components with perovskite structure were prepared *via* the sol-gel method and characterized by different techniques such as XRD, FTIR TEM and EDX. Moreover, an absorbance spectrum in UV region was applied to estimate the optical band gap energy and dependence of resistivity and electrical properties of the samples were studied.

2. Experimental

2.1. Synthesis

The perovskite precursors in this work were prepared by the citrate-based sol-gel method. Reagents of La_2O_3 (99.99 % purity), $CaCO_3$ (99.99 % purity), $Ni(NO_3)_2.6H_2O$ (99.99 % purity), $Co(NO_3)_2.6H_2O$ (99.99 % purity), citric acid (CA) (99.5 % purity) and nitric acid were used as starting materials. La_2O_3 and $CaCO_3$ weighed and dissolved in nitric acid to form lanthanum nitrate and calcium nitrate. Then the aqueous solutions of metal nitrates

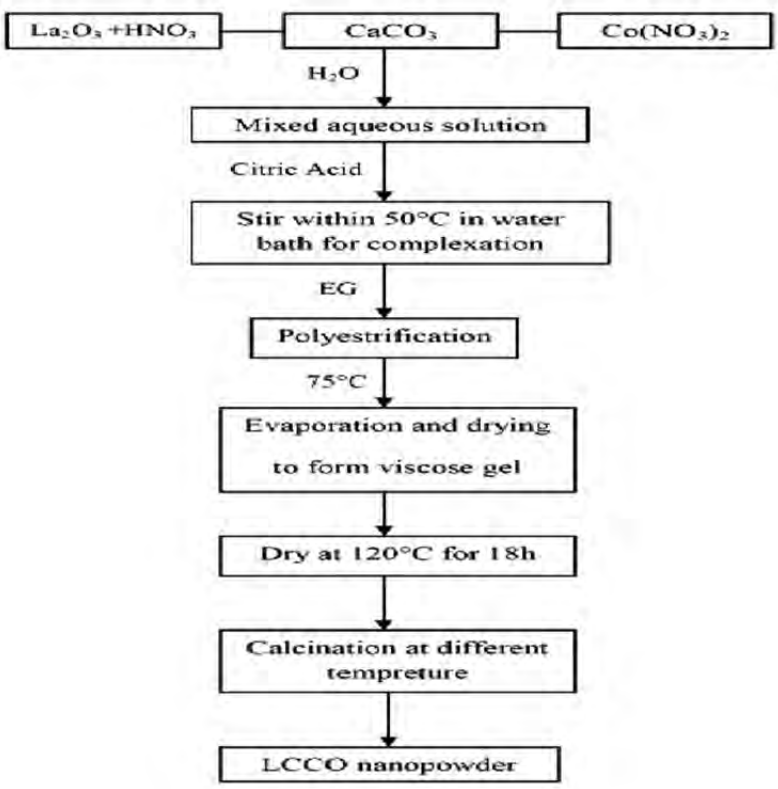

Figure 1 Flow chart of LCCO synthesis by the Pechini method.

with nominal atomic ratios La : Ca : Co = 0.5 : 0.5 : 1 (LCCO) and La:Ca:Ni = 0.5:0.5:1 (LCNO) were mixed together in deionized water. Citric acid was added proportionally to the metal solution to have the same amounts of equivalents. The solution was concentrated by evaporation at approximately 50 °C with stirring for 1 h to convert them to stable (La, Co, Ni)/CA complexes. Then EG was added to this solution as a cross-linking agent. The solution while being stirred, was heated at approximately 75 °C to remove excess water and subsequently to accelerate polyesterification reactions between CA and EG. During the evaporation of the solvent, reddish-brown gases corresponding to N_xO_y removed from the solution and a viscous and bubbly mass (the violet (LCCO) or green (LCNO) resins) was produced during cooling. Then, the dry gel was obtained by putting the sol into an oven and heated slowly to 100 °C for 6 h, The gel pieces were ground to form a fine powder. Finally, $La_{0.5}Ca_{0.5}CoO_{3-\delta}$ and $La_{0.5}Ca_{0.5}NiO_{3-\delta}$ nanoparticles were obtained by thermal treatment of the precursors at 650 °C and 750 °C for 9 h in air. The annealing of the amorphous precursor allowed to removing most of the residual carbon and the rhombohedral perovskite phase with the R-3m space group was obtained. A typical flow diagram for the preparation of LCCO by sol-gel processing is shown in Fig. 1. The procedure is the same for LCNO composition.

2.2. Characterization

Phase purity and crystal structure of the materials were determined by X-ray diffractometer (XRD). The measurements were obtained with a Rigaku D/MAX RB XRD using Cu Kα radiation (λ = 1.5418 Å and θ = 20–70°) at room temperature. Micrographs were recorded using LEO 912AB transmission electron microscope (TEM) under a working voltage of 120 kV. Specimens were prepared by dispersing small amounts of powder in ethanol. The visible and UV absorption spectra were measured using Agilent 8453 UV/VIS/NIR spectrophotometer in 200–800 nm spectral region. The FTIR transmission spectra in the region 400–4000 cm^{-1} were recorded for all samples using FTIR Nexus 670 by KBr pellet technique. The specific surface area (SSA) of the nanopowders was calculated using the BET method from the nitrogen adsorption isotherms obtained at 77 K on samples outgassed at 250 °C with the use of a Micromeritics Accusorb 2100E apparatus. Specific resistivity (ρ) was measured on pellets, pressed for 5 min into bars of 25 × 8 × 3 mm under 300 MPa pressure. In order to reduce their porosity and improve their adhesion, the samples were then sintered at 1100 °C for 4 h in air. The density of the sintered pellets, determined by Archimedes' method, was in the range 91–93 % of their theoretical value. The theoretical density of 6.23 and 6.59 g/cm^3 for, respectively, LCCO and LCNO, was calculated from the results of X-ray diffraction (XRD) studies.

Conducting silver paint was applied to both sides of the pellets. The specific resistivity value was calculated by Equation (2):

$$\rho = R\frac{A}{l}, \qquad (2)$$

where R is the measured sample resistance, A is the cross-section area and l is the thickness of the pellet. Absorption spectroscopy was used to calculate the band gap energy of nanoparticles, for this purpose, the nanoparticles were dispersed in distilled water using ultrasonic waves.

3. Results and Discussion

3.1. Thermal Characterization

Figure 2 shows the DTA curves of the LCCO and LCNO precursors obtained at a heating rate of 5 °C min^{-1} in air from room temperature to 1000 °C. The first weight loss occurs during the heating step from room temperature to 230 °C, which is due to the dehydration and decomposition of nitrates. DTA curves

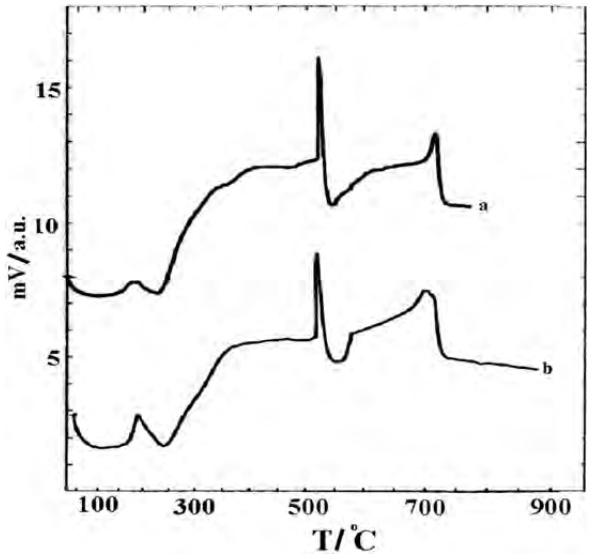

Figure 2 DTA curves of the as-synthesized (a) LCCO and (b) LCNO precursors.

illustrate two endothermic peaks at 120 °C and 230 °C. A weight loss of about 75 % is observed from 230 °C to about 530 °C, which corresponds to the oxidizing combustion of the organic compounds such as citric acid. These curves reveal a strong and sharp exothermic peak with a vertex at 520 °C which is likely due to the oxidation or combustion of the chelate complex along with forming the metal oxides. Between 530 °C and 720 °C, the DTA curves show both endothermic and exothermic peaks at 550 °C and 700 °C, respectively. These peaks may be attributed to the decomposition or solid state reaction of the carbonate intermediates. From 740 °C to 1000 °C, the DTA curves show no further endo- or exo-thermal peak, and very little weight loss is observed.

3.2. Structural Characterization

Fourier transform infrared spectra were obtained for xeogels and nanopowder samples after heating treatment leading to the oxides. Figs. 3 and 4 show the FTIR spectra of the LCCO and LCNO powders in the range of 600–4000 cm^{-1}, calcined at 650 °C and 750 °C for 9 h in air and fresh xerogels. The FTIR spectrum is similar to the most other ABO_3-type perovskite compounds which have common BO_6 oxygen-octahedral structure.[24–26] Two samples show the typical M–O–C pair vibrations around 1410 and 1590 cm^{-1}.[27] The characteristic bands at about 1700 and 1250 cm^{-1} correspond to the H–O–H bending vibration[28] of the residual water and the anti-symmetric NO_3^- stretching vibration,[29] respectively. A broad band is observed between 3400 and 3500 cm^{-1} corresponds to the O–H stretching vibration[30] due to water species occluded into the gel. An intermediate absorption band is observed at 1070 cm^{-1} and corresponded to C–O bond.[31]

The FTIR spectra of calcined samples show the vanishing of bands related to organic and hydroxyl groups. Several broad bands are observed at 500–700 cm^{-1} in the far IR spectra of two samples, one of them is strong at ~ 590 cm^{-1} and other weak peaks at 402 and 324 cm^{-1} for LCCO or 460 and 265 cm^{-1} for LCNO (Fig. 5). These peaks are characteristics of perovskite oxides and can be attributed to υM–O stretching and δO–M–O bending mode of vibrations, respectively.[32–34] These observed infrared peaks are composition of υ_1-BO_6 (B = Co, Ni) stretching normal vibration modes along the spontaneous polarization in these structures.

The XRD patterns for the heat treated LCCO and LCNO powders are shown in Figs. 6 and 7, respectively. Samples were heat treated at 650 and 750 °C for 9 h in air (heating rate: 3 °C min^{-1}) after previously dwelling at 100 °C for 6 h.

The XRD results reveal the existence of a perovskite-type phase for sol-gel method at all temperatures. The structural results for LCCO and LCNO in this work are summarized in Table 1. As Fig. 6 shows, $La_{0.5}Ca_{0.5}CoO_{3-\delta}$ exhibits a crystalline perovskite phase (ABO_3) with relevant diffraction peaks properly indexed. In this figure, we can identify the presence of (0 1 2), (1 1 0), (2 0 2), (0 2 4), (1 1 6), (2 1 4) and (2 2 0) crystal planes of metallic hexagonal-rhombohedral structure for LCCO (JCPDS-36-1390). In comparison with the previous results for $LaCoO_3$,[35] formation of the perovskite phase starts at 650 °C. At higher temperatures, the increase in the intensity of the crystalline diffraction lines is observed. In Fig. 7, the diffraction peaks at 2θ angles appear at 24.41°, 33.24°, 41.16°, 47.64°, 54.2°, 58.44°, and

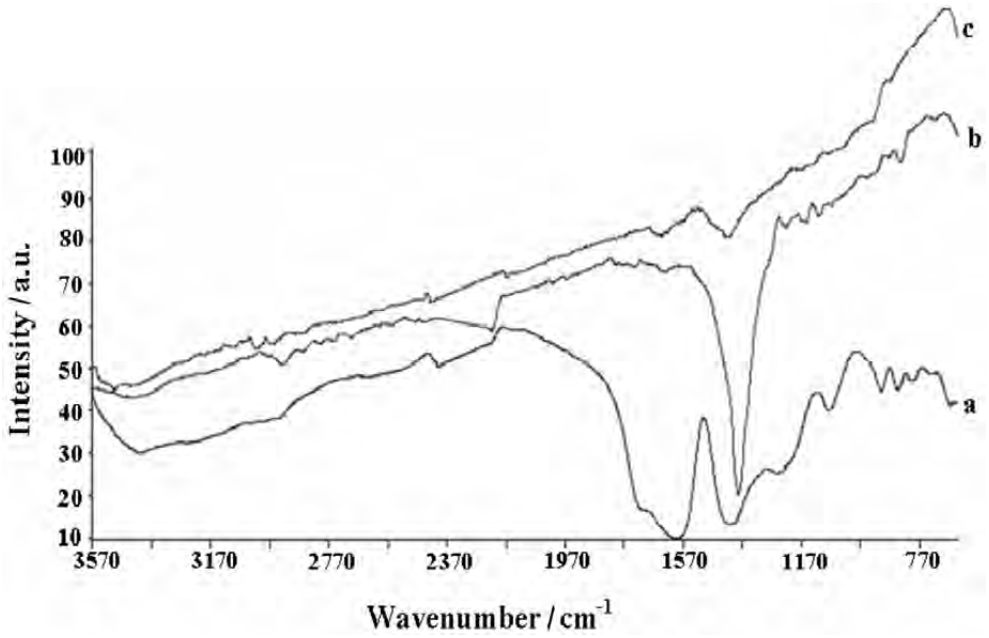

Figure 3 IR spectra of LCCO (a) fresh xerogel, (b) the calcined powders at 650 °C and (c) at 750 °C for 9 h in air.

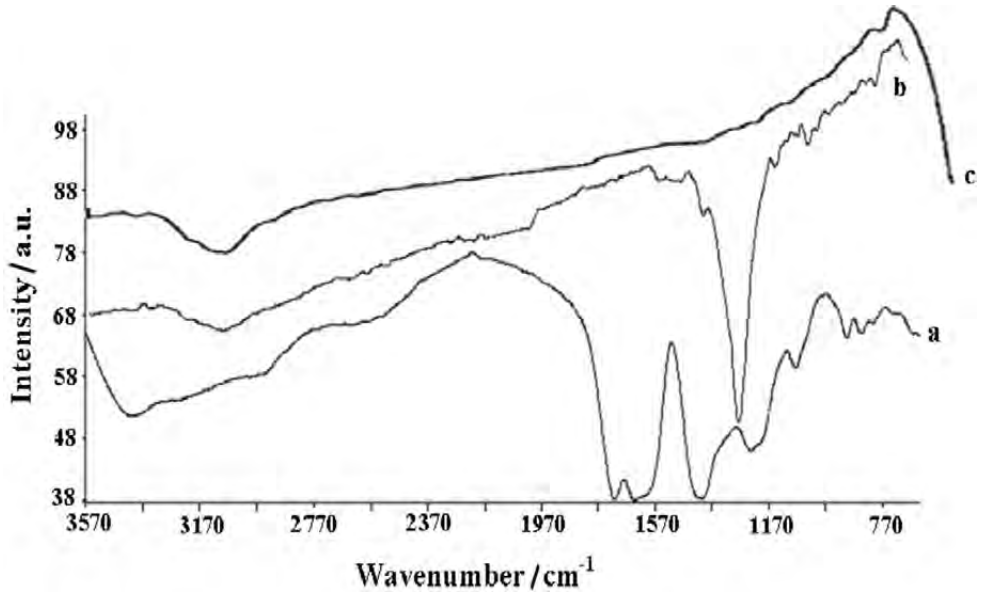

Figure 4 IR spectra of LCNO (a) fresh xerogel, (b) the calcined powders at 650 °C and (c) at 750 °C for 9 h in air.

69.76° can be assigned to scattering from the (1 0 1), (1 1 0), (1 1 4), (2 0 0), (1 1 6), (0 0 8) and (2 2 0) planes of the $La_{0.5}Ca_{0.5}NiO_{3-\delta}$ perovskite type crystal lattice, respectively.

The crystallite grain size of the monophase samples was determined from the full width at half-maximum width (FWHM) of the XRD (1 1 0) peak using the Scherrer formula:

$$D_{hkl} = \frac{0.9\lambda}{\beta_{hkl}\cos\theta_{hkl}} \quad (3)$$

where D_{hkl} is the particle grain size perpendicular to the normal line of (h k l) plane, β_{hkl} is the full width at half maximum, θ_{hkl} is the Bragg angle of (h k l) peak, and λ is the wavelength of X-ray. The results indicate that LCCO and LCNO powders sizes calcinated at 750 °C are ~ 30 and ~ 40 nm, respectively.

Figure 8 shows typical TEM images of nanosized $La_{0.5}Ca_{0.5}CoO_{3-\delta}$ and $La_{0.5}Ca_{0.5}NiO_{3-\delta}$ calcined at 750 °C prepared by the modified Pechini sol-gel method. The size of nanoparticle

Table 1 Structural result for LCCO and LCNO nanopowders calcinated at 750 °C for 9 h in air.

Nanopowders	2θ/°	(hkl)	Structure	Lattice parameter/Å	Space group	Volume/Å ^{3}
LCCO	23.24	(012)	Hexagonal (Rh)	a = b = 5.446		
	33.18	(110)		c = 13.111	R-3m (166)	336.761
	40.85	(202)		$\alpha = \beta = 90$		
	47.62	(024)		$\gamma = 120$		
	59.09	(214)				
LCNO	24.41	(101)	Hexagonal (Rh)	a = b = 4.866		
					R-3m (166)	294.812
	33.24	(110)		c = 12.652		
	41.16	(114)		$\alpha = \beta = 90$		
	47.64	(200)		$\gamma = 120$		
	58.44	(008)				

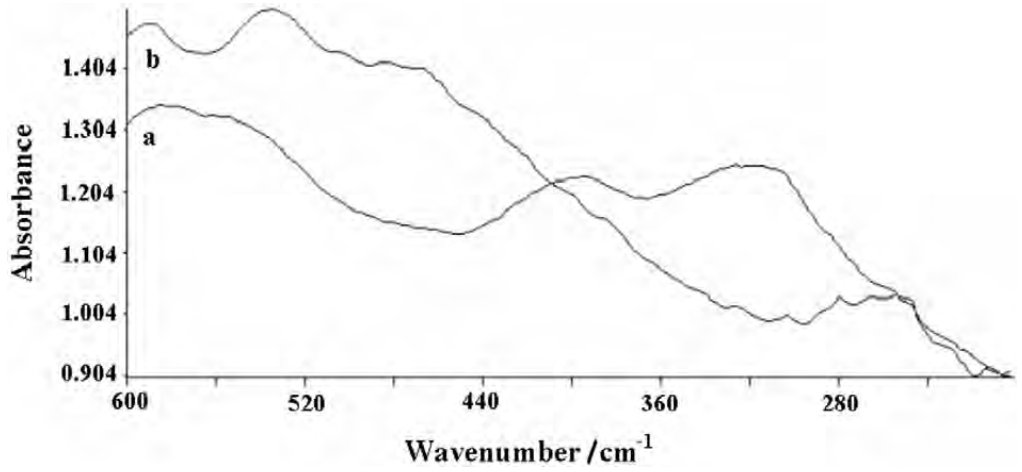

Figure 5 Far-IR spectrum of (a) LCCO and (b) LCNO nanoparticles.

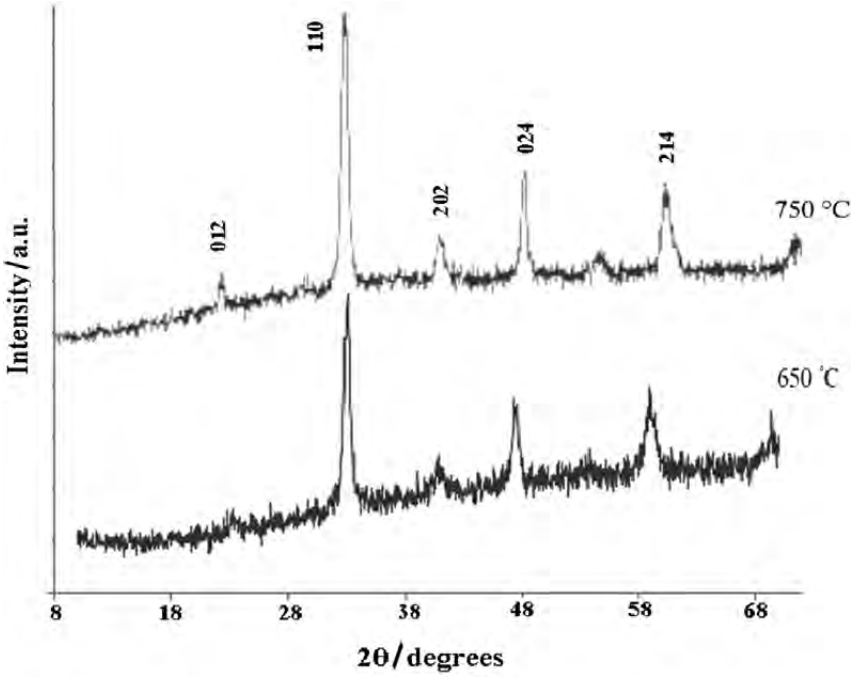

Figure 6 XRD patterns of samples of the LCCO nanopowder calcinated at different temperatures of 650 °C and 750 °C.

of LCCO sample is in the range of 25 to 32 nm. Due to the high temperature during the combustion process, there are some aggregates. As is obvious from this image, the range of particles size of LCNO sample is 32 to 40 nm. These values are in agreement with the result achieved from XRD measurement.

Based on the SEM images, the surface looks rough and nearly fully covered with the particles grown on it. Also the existence of lanthanum, calcium, cobalt and oxygen in LCCO and lanthanum, calcium, nickel and oxygen in LCNO was confirmed by SEM-EDX analysis (Fig. 9).

The specific surface area was measured by the Brunauer-Emmett-Teller (BET) method and the results are given in Table 2.

Table 2 The specific surface area of samples calcined at 750°C for 9 h in air.

Sample	SSA/m^2 g^{-1}	Uncertainty
LCCO	7.98	±0.08
LCNO	6.91	±0.02

The specific surface area of LCNO is lower than LCCO. These values are in agreement with TEM results that reveal LCCO sample is smaller than LCNO.

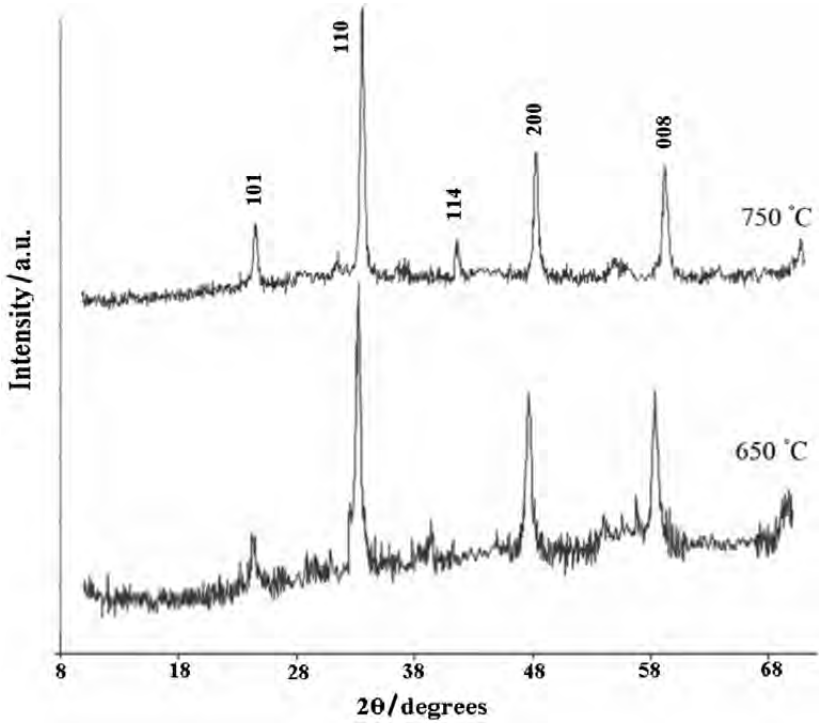

Figure 7 XRD patterns of samples of the LCNO nanopowder calcinated at different temperatures of 650 °C and 750 °C.

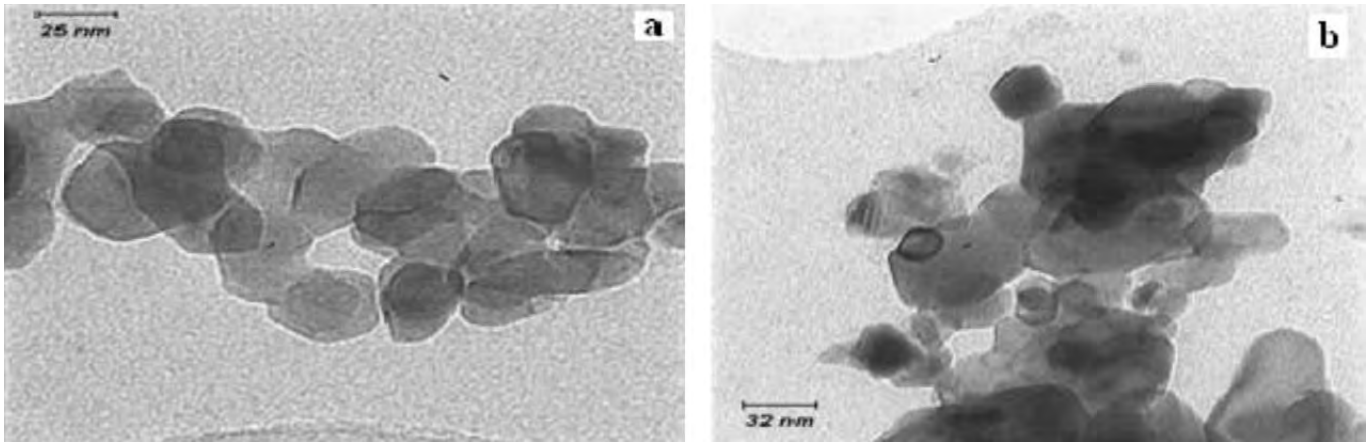

Figure 8 TEM micrograph of nanopowders at 750 °C (**a**) LCCO and (**b**) LCNO nanoparticles.

3.3. Electrical and Optical Properties

Figure 10 displays the temperature dependence of the specific electrical resistivity of $La_{0.5}Ca_{0.5}CoO_{3-\delta}$ and $La_{0.5}Ca_{0.5}NiO_{3-\delta}$, respectively, which were sintered at 1100 °C at air for 4 h, and then slowly cooled within l0–15 h at room temperature. These samples were essentially equilibrated with air oxygen. Since the Ni doping increases the value of resistivity much more rapidly than other 3d metals,[36] comparing the two graphs shows that the specific electrical resistivity of LCCO at ambient temperature is significantly smaller than that of LCNO. In both compositions, the resistance decreases exponentially with increasing temperature which is a typical semiconductor behaviour.[37] The electrical conductivity mechanism of perovskite oxides has been discussed by several authors. According to their investigations, charge transfer occurs *via* the M–O–M bonds due to the exchange of the electronic state of the transition metal between M^{+4} and M^{+3}.[38,39]

Figure 11 shows the measured resistivity and reciprocal

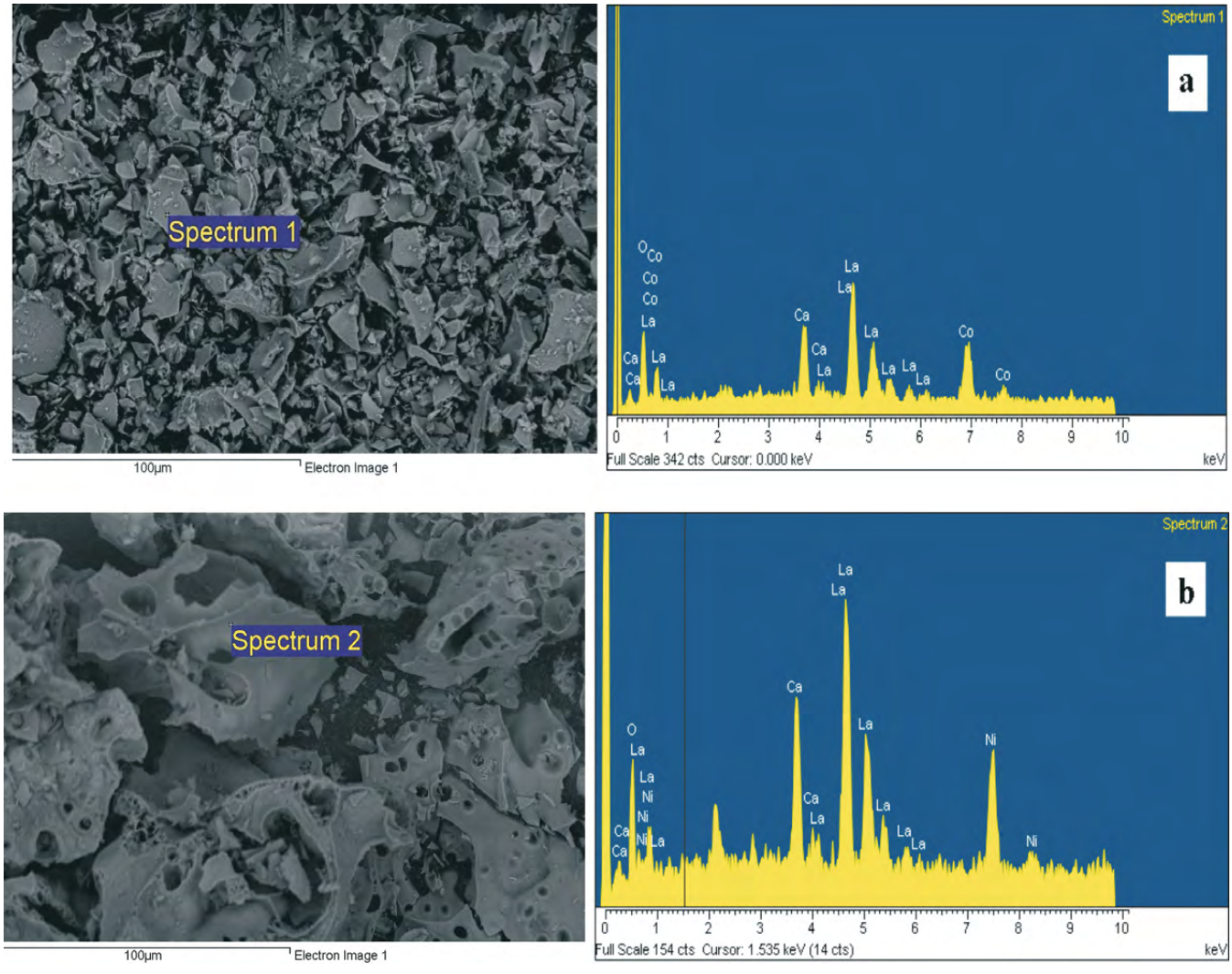

Figure 9 SEM-EDX images of (**a**) LCCO and (**b**) LCNO nanoparticles.

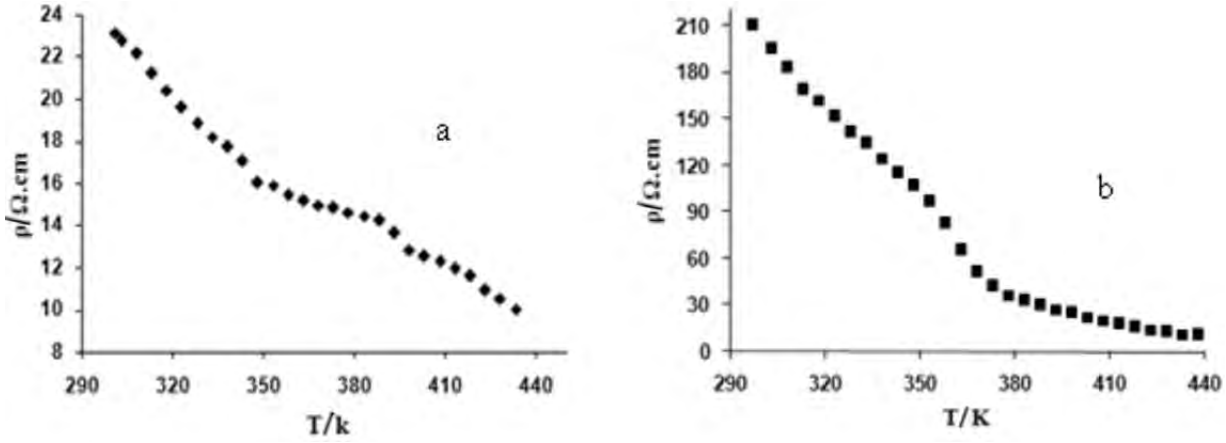

Figure 10 Temperature variation of specific resistivity. (**a**) LCCO and (**b**) LCNO samples.

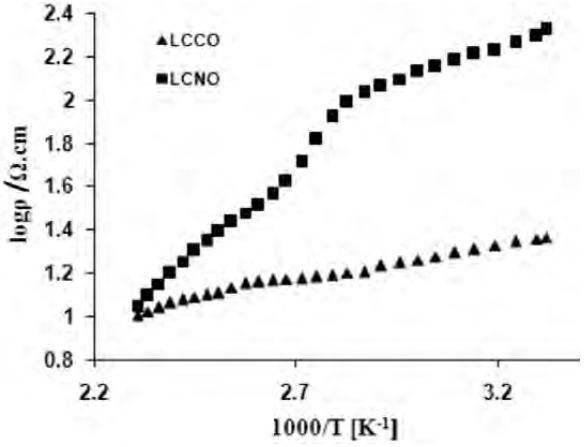

Figure 11 Plots of the log ρ *versus* 1/T for LCCO and LCNO nanoparticles.

temperature (1/T) of the samples. The increase of the electrical conductivity with the temperature shows that the compounds are semiconductor, whereas, linearity between logρ and (1/T) indicates that the mobility is thermally activated as expected for small polaron hopping.

Calculating the absorption coefficients (α) of the synthesized powders in the strong absorption region needs both the transmission and reflection spectra. In this study, the UV spectrum was used to calculate the absorption coefficient as a function of photon energy (hυ). The square of absorption coefficient, α^2, as a function of photon energy (hυ) is shown in Fig. 12. It must be noted that the absorbance behaviour is completely different from the thin films due to scattering process of the ultraviolet wave from particles dispersed in water. Since the absorbance values of two materials were strong, the absorption coefficient was evaluated from Lambert's principle at various wavelengths. The relationship between the absorption coefficient and the optical band gap for direct allowed transition is expressed from the Equation (4):

$$(\alpha h\upsilon)^2 = C(h\upsilon - E_g), \quad (4)$$

where C is an energy-independent constant. By plotting $(\alpha h\upsilon)^2$ *versus* hυ, values of the optical band gap (E_g) can be calculated from the extrapolated linear portion of the plot for the two samples. According to Fig. 12, the optical band gaps energy for LCCO and LCNO are approximately equal to 5.95 and 5.57 eV, respectively. The value of E_g for LCNO sample is smaller than LCCO which indicates optical band gaps of the samples decrease when Ni is replaced with Co in the perovskite structure.[40]

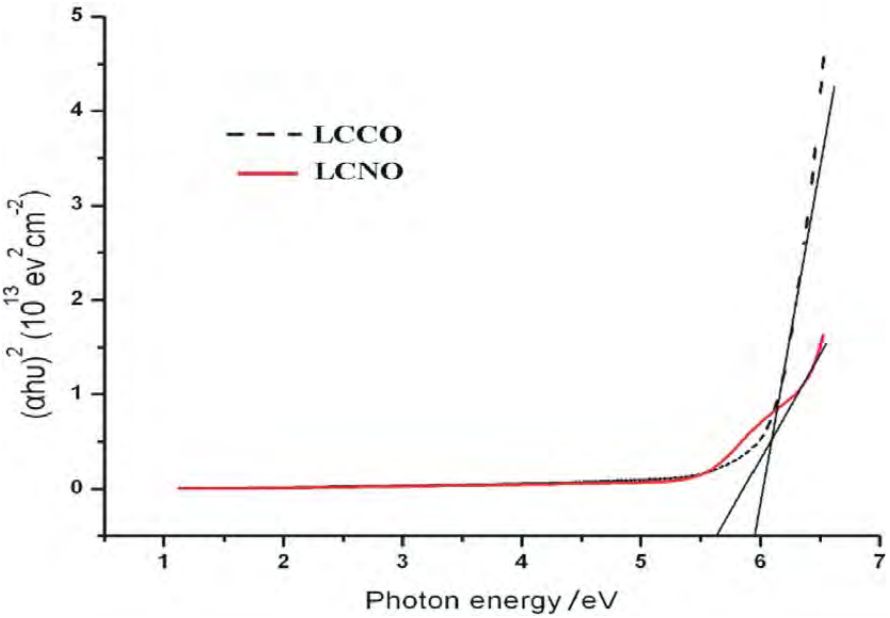

Figure 12 Dependence of the absorption coefficients $(\alpha h\upsilon)^2$ on the photon energy for LCCO and LCNO nanopowders.

4. Conclusions

The nanopowders of $La_{0.5}Ca_{0.5}CoO_{3-\delta}$ and $La_{0.5}Ca_{0.5}NiO_{3-\delta}$ were synthesized by the sol-gel method using citric acid and ethylene glycol as a complexing reagent and a cross-linking agent, respectively. DTA curves reveal that the amount of pyrochlore phase decreased at 550 °C and disappeared at 700 °C. The XRD patterns and TEM images reveal that the nanoparticles were prepared at different calcinated temperatures (650 °C and 750 °C) for 9 h and there is a good crystallinity with hexagonal (Rh) phase for both LCCO and LCNO components. The nanoparticles exhibit a regular morphology with homogeneous particle size distribution. The IR spectra also confirm the structure of prepared nanoparticles. The specific electrical resistivity of the $La_{0.5}Ca_{0.5}MO_3$ (M = Co and Ni) were studied in the temperature range of 25 to 170 °C. The optical band gap of the LCCO and LCNO was evaluated using the UV spectroscopy. The significant changes in the band-gap energy values are as a result of grain growth and optical nature of transition metal cations. The band gaps of the precursors decrease when Ni is replaced with Co in the structure. This result is similar to the phenomenon in the semiconductor alloys.

Acknowledgements

The authors wish to thank the financial support of Ferdowsi University of Mashhad for this project (P439) and are grateful to Materials and Electroceramics Laboratory of department of physics for electrical measurements. We also acknowledge R. Pesian and N. Hashemian for taking TEM images and EDX analysis at the central lab of Ferdowsi University of Mashhad.

References

1 Z. Gao and R. Wang, *Appl. Catal. B: Environ.*, 2010, **98**, 147–153.
2 J. Gao, F.X. Hu and H. Yao, *Appl. Surf. Sci.,* 2006, **252**, 5521–5524.
3 Q.G. Chi, W.L. Li, Y. Zhao, and W.D. Fei, *J. Sol-Gel Sci. Technol.*, 2010, **54**, 286–291.
4 Z. Brankovic, K. Duris, A. Radojkovic, S. Bernik, Z. Jaglicic, M. Jagodic, K. Vojisavljevic and G. Brankovic, *J. Sol-Gel Sci. Technol.*, 2010, **55**, 311–316.
5 Y.D. Zhen, S.P. Jiang, S. Zhang and V. Tan, *J. Eur. Ceram. Soc.,* 2006, **26**, 3253–3264.
6 S.P. Jiang, *J. Mater. Sci.*, 2008, **43**, 6799–6833.
7 I. Krkljus, Z. Brankovic, K. Djuris, V. Vukotic, G. Brankovic and S. Bernik, *Int. J. Appl. Ceram. Technol.,* 2008, **5**, 548–556.
8 B.A. Van Hassel, T. Kawada, N. Sakai, H. Yokokawa, M. Dokiya and H.J.M. Bouwmeester, *Solid State Ionics,* 1993, **66**, 41–47.
9 Z. Hu, Y. Yang, X. Shang and H. Pang, *Mater. Lett.* 2005, **59**, 1373–1377.
10 T. Hirano, H. Purwanto, T. Watanabe and T. Akiyama, *J. Alloys Compd.*, 2007, **441**, 263–266.
11 P.M. Woodward, *Acta Crystall. B,* 1997, **53**, 44–66.
12 K. Tezuka, Y. Hinatsu, A. Nakamura and T. Inami, *J. Solid State Chem.*, 1998, **141**, 404–410.
13 A.J. Zhou, T.J. Zhu and X.B. Zhao, *Mater. Sci. Eng. B,* 2006, **128**, 174–178.
14 V. Szabo, M. Bassir, A. VanNeste and S. Kaliaguine, *Appl. Catal. B: Environ.*, 2002, **37**, 175–180.
15 S. Nakayama, M. Okazaki, Y.L. Aung and M. Sakamoto, *Solid State Ionics,* 2003, **158**, 133–139.
16 V.V. Srdic, R.P. Omorjan and J. Seydel, *Mater. Sci. Eng. B,* 2005, **116**, 119–124.
17 N.P. Bansal and Z. Zhong, *J. Power Sources,* 2006, **158**, 148–153.
18 D. Berger, V. Fruth, I. Jitaru and J. Schoonman, *Mater. Lett.*, 2004, **58**, 2418–2422.
19 D. Berger, C. Matei, F. Papa, G. Voicu and V. Fruth, *Prog. Solid State Chem.*, 2007, **35**, 183–191.
20 M. Pechini, US Patent (1967) No. 3,330,697.
21 S. Cizauskaite and A. Kareiva, *Cent. Europ. J. Chem.*, 2008, **6**, 456–464 .
22 N.L. Petrova, D.S. Todorovsky and V.G. Vasileva, *Cent. Europ. J. Chem.*, 2005, **3**, 263–278.
23 P. Song, Q. Wang and Z. Yang, *Sensors and Actuators B,* 2009, **141**, 109–115.
24 E.R. Leite, C.M.G. Sousa, E.Longo and J.A. Varela, *Ceram. Int.*, 1995, **21**, 143–152.
25 W. Nimmo, N.J. Ali, R.M. Brydson, C. Calvert, E. Hampartsoumian, D. Hind and S.J. Milne, *J. Am. Ceram. Soc.*, 2003, **86**, 1474–1480.
26 A. Sakar-Deliormanl, E. Celik and M. Polat, *Ceram. Int.*, 2009, **35**, 503–508.
27 J. Kim and I. Honma, *Electrochim. Acta,* 2004, **49**, 3179–3183.
28 M. Sadakane, T. Horiuchi, N. Kato, C. Takahashi and W. Ueda, *Chem. Mater.*, 2007, **19**, 5779–5785.
29 S. Liu, X. Qian and J. Xiao, *J. Sol-Gel Sci. Technol.*, 2007, **44**, 187–193.
30 P.N. Kuznetsov, L.I. Kuznetzova, A.M. Zhyzhaev, G.L. Pashkov and V. V. Boldyrev, *Appl. Catal. A,* 2002, **227**, 299–307.
31 K. Nakamoto, *Infrared and Raman Spectra of Inorganic and Coordination Compounds,* Plenum Press, New York, 1978.
32 D.A, Neumayer and E.J. Cartier, *Appl. Phys.*, 2001, **90**, 1801–1808.
33 Y. Hao, J. Li, X. Yang, X. Wang and L. Lu, *Mater. Sci. Eng. A, 2004,* **367**, 243–247.
34 R.N. Singh and B. Lal, *Int. J. Hydrogen Energy,* 2000, **27**, 45–55.
35 N.A. Merino, B.P. Barbero, P. Grange and L.E. Cadus, *J. Catal.*, 2005, **231**, 232–244.
36 Z. Mao, G. Xu, H. Yan, B. Wang, X. Qiu and Y. Zhang, *Phys. Rev. B,*1998, **58**, 15116–15119.
37 A.J. Zhou, T.J. Zhu and X.B. Zhao, *Mater. Sci. Eng. B,* 2006, **128**, 174–178.
38 N. Fujihira, T. Sei and T. Tsuchiya, *J. Sol-Gel Sci. Technol.*, 1995, **4**, 135–140.
39 M. Losurdo, A. Sacchetti, P. Capezzuto, G. Bruno, L. Armelao, D. Barreca, G. Bottaro, A. Gasparotto, C. Maragno and E. Tondello, *Appl. Phys. Lett.*, 2005, **87**.
40 J. Yang, T. Zhang, M. Ni, L. Ding and W.F. Zhang, *Appl. Surf. Sci.*, 2009, **256**, 17–20.